Contents lists available at ScienceDirect

Journal of Chromatography A

journal homepage: www.elsevier.com

Sedimentation field flow fractionation and optical absorption spectroscopy for a quantitative size characterization of silver nanoparticles

Catia Contado [a,*], Roberto Argazzi [b], Vincenzo Amendola [c]

[a] Department of Chemical and Pharmaceutical Sciences - University of Ferrara, Via Fossato di Mortara, 17 - 44121 Ferrara, Italy
[b] ISOF-CNR c/o Department of Chemical and Pharmaceutical Sciences - University of Ferrara, Via Fossato di Mortara, 17 - 44121 Ferrara, Italy
[c] Department of Chemical Sciences - University of Padova, Via Marzolo 1 - 35131 Padova, Italy

ARTICLE INFO

Article history:
Received 30 June 2016
Received in revised form 4 October 2016
Accepted 11 October 2016
Available online xxx

Keywords:
Silver nanoparticles
Sedimentation field flow fractionation
Optical absorption spectroscopy (OAS)
Surface plasmon resonance (SPR)
Mie theory
Particle size distribution

ABSTRACT

Many advanced industrial and biomedical applications that use silver nanoparticles (AgNPs), require that particles are not only nano-sized, but also well dispersed, not aggregated and not agglomerated. This study presents two methods able to give rapidly sizes of monodispersed AgNPs suspensions in the dimensional range of 20–100 nm.

The first method, based on the application of Mie's theory, determines the particle sizes from the values of the surface plasmon resonance wavelength (SPR_{MAX}), read from the optical absorption spectra, recorded between 190 nm and 800 nm. The computed sizes were compared with those determined by transmission electron microscopy (TEM) and dynamic light scattering (DLS) and resulted in agreement with the nominal values in a range between 13% (for 20 nm NPs) and 1% (for 100 nm NPs),

The second method is based on the masterly combination of the Sedimentation Field Flow Fractionation (SdFFF − now sold as Centrifugal FFF-CFFF) and the Optical Absorption Spectroscopy (OAS) techniques to accomplish sizes and quantitative particle size distributions for monodispersed, non-aggregated AgNPs suspensions. The SdFFF separation abilities, well exploited to size NPs, greatly benefits from the application of Mie's theory to the UV–vis signal elaboration, producing quantitative mass-based particle size distributions, from which trusted number-sized particle size distributions can be derived. The silver mass distributions were verified and supported by detecting off-line the Ag concentration with the graphite furnace atomic absorption spectrometry (GF-AAS).

1. Introduction

Silver nanoparticles (AgNPs), for their broad spectrum of antibacterial and fungicidal activities, are active constituents of a number of consumer products, including soaps, pastes, cosmetics, plastics, food packaging, textiles, wound dressings, biomedical devices and many others. AgNPs have also unique optical, electrical, and thermal properties that make them suitable to be incorporated into products that range from photovoltaics to biological and chemical sensors, such as conductive inks, pastes and fillers, photonic devices such as, for example, solar cells where AgNPs are used as plasmonic light traps. The economic interests around AgNPs are consequently important, as they are their market horizons.

AgNPs with different morphologies, sizes, and shapes to target specific applications can be nowadays easily synthetized; nevertheless, one of the critical criteria that has to be satisfied remains the size distribution that should be often as narrow as possible. This requirement has determined an increasing attention towards all those analytical methods, which are potentially able to give this information.

The family of analytical techniques termed Field-Flow Fractionation (FFF) has entered in the laboratory practice as a set of methods suitable to separate and characterize nano and micro particles, colloids, macromolecules, natural and synthetic polymers [1,2]. They are elution techniques, in which the detection varies depending on the method and the sample type. Common detectors might be UV–vis optical absorption spectrophotometer (OAS), multi-angle laser light scattering (MALLS), dynamic light scattering (DLS), refractive index (RI), or destructive detectors such as the graphite furnace atomic absorption spectrometer (GF-AAS), the inductively coupled plasma atomic emission spectrometer (ICP-AES) or the inductively coupled plasma mass spectrometer (ICP-MS).

The Sedimentation FFF (SdFFF), and the Flow-FFF (F4) techniques are both suitable to analyze gold [3,4] and silver NPs [5–8]. For these specific applications, the simplest instrumental configuration involves the use of an UV–vis detector and an aqueous solvent as eluent medium. The analysis result is represented graphically by a fractogram (elugram), where the detector response is reported as a function of the analysis time (retention time). From these data is possible to derive the particle size distribution (PSD) of the sample. However, the conversion of the fractogram into the PSD hides an important assumption connected to the proportionality between the detector signal and the sample concentration or the sample mass.

The linearity between the absorbance and the sample concentration, almost obvious for absorbing molecular species, becomes indeed more complicated in the case of particulate species, where the light scattering component adds to the absorbing component [9]. The

* Corresponding author.
Email addresses: kat@unife.it, catia.contado@unife.it (C. Contado); roberto.argazzi@unife.it (R. Argazzi); vincenzo.amendola@unipd.it (V. Amendola)

http://dx.doi.org/10.1016/j.chroma.2016.10.026
0021-9673/

absorption component remains mass proportional, while the scattering component follows complicated relations, which depend on the particle size (diameter *d*) compared with the incident electromagnetic wavelength λ [9]. The use of Mie's theory in the FFF literature is limited to the cases in which the particle turbidity (scattering) was evaluated under the conditions that the ratio between the scattering coefficient and the particle diameter was constant and the refractive index of the sample was known [10,11].

The UV–vis signal of plasmonic NPs, such as the AgNPs, is by far more complicated, because both absorption and scattering of light depends in a nontrivial way on particles' size, shape, aggregation, dielectric environment, surface coating and even mutual electromagnetic interaction in nearby particles [12–14]. These correlations complicate the expressions describing the dependence of the OAS signal on NPs' concentration.

This study demonstrates firstly that the correct application of Mie's theory allows to determine quite rapidly and with a reasonable degree of accuracy the size of AgNPs aqueous suspensions, from the OAS spectra. The reliability of the evaluation is assessed by comparing the NP sizes, here comprised in the range 20–100 nm, with those achieved with other analytical techniques, such as transmission electron microscopy (TEM) and DLS [7]. Secondly, that the coupling on-line of the UV–vis detector (OAS) with a SdFFF allows to get a quantitative particle size distribution. This is possible since the SdFFF provides an independent and accurate determination of spherical particles' diameter from the measurement of the retention time, while the on-line OAS provides a signal that through the Mie's theory is related to the relative silver abundance of each size. The quantitative mass-based particle size distributions, elaborated from the fractograms, are therefore converted in number-sized PSD. The exactness of the quantitative PSD profiles is verified by the off-line silver amount determination provided by the graphite furnace atomic absorption spectrometer (GF-AAS).

2. Theory

2.1. OAS spectrum modeling

Optical properties of AgNPs were calculated with Mie's theory, which is based on the solution of the Maxwell's equations in spherical coordinates using the multipoles expansion of the electric and magnetic fields and accounting for the discontinuity of the dielectric constant between the sphere and the surrounding medium [9]. Detailed information about the procedures are reported in the paragraph *SM-2* of the Supplementary material (SM).

2.2. SdFFF-OAS coupling

The theory of SdFFF, is widely documented in literature [15–17]. However, for the sake of discussion, the paragraph *SM-4* in the Supplementary material reports the fundamental relationships which govern the retention, the proportionality of the retention time with the particle sizes, and how, for a flow-through analysis, the optical absorbance and the extinction cross section σ_{ext} are used to get quantitative particle size distributions (mass or number frequency function $F_{m,i}$, $F_{n,i}$).

3. Materials and methods

3.1. Reagents

Nearly monodisperse sodium citrate stabilized silver AgNPs dispersions of 20, 30, 40, 60, 70 and 100 nm at a nominal concentration of 20 mgL^{-1} were kindly donated by the Joint Research Centre, Institute for Health and Consumer Protection, Ispra (Italy). To avoid silver particle degradation or precipitation, dispersions were stored at 4 °C and protected from prolonged exposure to light.

Information regarding the sizes and the actual total silver concentrations, determined with complementary techniques by the JRC are reported in Tables 1 and 2 respectively.

NaOH and sodium citrate (Carlo Erba Reagents − Italy) were used to prepare the mobile phase (eluent) for the SdFFF instrument.

All solutions were prepared using ultrapure deionised water (18 MΩ cm^{-1}) obtained from a MilliQ system (Merck Millipore Milan, Italy).

3.2. SdFFF

A Colloid/Particle Fractionator SdFFF system (Model S101 Postnova Analytics, Landsberg, Germany), described in detail elsewhere [3,18], was employed to fractionate the AgNPs according to their buoyant mass. AgNP suspensions were injected through a 50 μL

Table 1
Sizes information about the AgNPs given by the suppliers and measured with different techniques and theoretical approaches. *The TEM sizes were chosen as the most reliable.

	Size (nm)					
	AgNP20	AgNP30*	AgNP40	AgNP60	AgNP70	AgNI
Nominal	20	30	40	60	70	100
TEM*	19.6 ± 1.6	32.3 ± 3.2	40.6 ± 3.0	57.4 ± 4.0	68.4 ± 4.2	99.4 ±
DLS [7]	25	45	54	67)	69	98
Mie Fit − Palik	10	46	48	64	74	102
Mie Fit − J&C	60	60	62	74	80	106
SPR_{MAX} − Palik	33	40	44	61	69	99
*Relative Error%	65	25	7	7	1	–
SPR_{MAX}− J&C	49	54	58	71	79	107
*Relative Error%	49	69	41	24	16	8

Table 2
Optical information evaluated from the UV–vis spectra, recorded on the samples "as received". The cell path was 1 cm. Ag atomic concentrations measured by ICP-MS data are the average on 3 replicate measurements. The Ag atomic concentrations computed by OAS are the average of 8 values, determined at 8 different wavelengths selected between 250 and 440 nm; data are reported as the average ± standard deviation.

	AgNP20	AgNP30	AgNP40	AgNP60	AgNP70	AgNP100
α @ 420 nm (L mg^{-1})	0.07553	0.08319	0.08118	0.07191	0.05989	0.03156
λ_{max} (nm)	401	410	415	429	441	493
Abs @ 420 nm	1.4426	1.4298	1.4856	1.3951	1.2637	0.5902
Ag atomic concentration ICP-MS* (mM) [7]	0.177	0.167	0.170	0.180	0.196	0.173
Average Ag atomic concentration Mie theory − Palik constant (mM)	0.202 ± 0.062	0.133 ± 0.041	0.151 ± 0.028	0.166 ± 0.030	0.191 ± 0.021	0.173 ± 0.011

Rheodyne loop valve. Particle elution was monitored by an UV–vis absorption detector Spectra SERIES UV100 (Thermo Separation Products, USA) operating at a fixed wavelength of 420 nm, equipped with a 3 mm flowcell optical path. An additional UV–vis photodiode array detector (four channel UVD 340U Dionex, Dionex GmbH Germering, Germany) was connected to the SdFFF in sequence after the first detector and set to monitor the sample elution at 275, 375, 400 and 420 nm. Its flowcell of 10 μL had an optical path of 9 mm. A Sykam S 1125 HPLC Pump (Sykam GmbH, Germany) was used to deliver the eluent. The SdFFF instrument was controlled by SPIN 1409, a program also used to acquire the fractrograms. The registered data were processed by FFF ANALYSIS (Postnova), to convert automatically the retention time in particle size, knowing the particle bulk density. For all AgNPs, the particle bulk density was set at 10.49 g cm^{-3} [19].

The eluent was a 10^{-5} M solution of sodium citrate in 18.2 mΩ cm^{-1} deionized water, basified at pH 9.2-9.3 with NaOH, freshly prepared each day, flowing at 0.7, 1 or 2 mL min^{-1} depending on the sample sizes. To ensure an uniform fractionating power over the wide range of particle diameters, spinning power gradients were used [20].

3.3. UV–vis − OAS

UV–vis spectra were recorded at room temperature in the 190–800 nm range with a Cary 300 UV–vis spectrophotometer (Agilent Technologies) using 1 cm path length quartz cuvettes, scan rate of 300 nm min^{-1} and data interval of 1 nm. The standard solutions were analyzed as received or diluted with deionized water 1:50. 18.2 mΩ cm^{-1} deionized water was used as a reference.

3.4. Calculations

All algorithms were developed under Wolfram Mathematica 6.0. The first (Algorithm#1) was developed for the evaluation of AgNPs size from optical absorption (Mie Fit). In this case, the model performed the optimal fitting of experimental UV–vis spectra with Eqs. (S1–S7) by using the average AgNPs size as the only parameter. Experimental spectra were fitted in the 250–800 nm spectral range, by varying d of 0.1 nm. A χ^2 fitting on a point every 5 nm was used for the calculation of the best spectra, which were normalized on the SPR maximum (SPR_{MAX}). Calculated curves were allowed to shift of 1 point, if necessary, to improve the matching with the position of the experimental SPR_{MAX}. Scaling the values of the calculated spectra to the experimental ones allows the determination of the concentration of the NPs, according to Eqs. (S20)–(S21).

A second algorithm (Algorithm#2) was written to estimate the extinction cross section σ_{ext} of AgNPs of predetermined size with Mie's theory and the results exploited for the evaluation of AgNPs concentration according to Eqs. (S20)-(S21), on the basis of experimentally measured absorbance.

A third algorithm (Algorithm#3) was developed to convert SdFFF fractograms into AgNPs or atomic Ag concentration. In this case, the input (absorbance versus AgNPs size, computed through the FFF theory) was transformed in concentration versus size by calculating first the $\sigma_{ext}(d,\lambda)$ with Mie's theory and subsequently the concentrations with Eqs. (S19)–(S22). The other input parameters required by the program are the refractive index of the dispersing medium (water, $n = 1.334$) and the optical path of optical absorption measurements (3 mm or 9 mm in the present case).

4. Results and discussion

AgNPs exhibit a strong UV–visible extinction band, size-dependent, known as localized surface plasmon resonance (SPR) that is not present in the spectrum of the bulk metal. SPR excitation results in wavelength-selective absorption with extremely large molar extinction coefficients ($\sim 3 \times 10^{11}$ M^{-1} cm^{-1}), resonant Rayleigh scattering with efficiency equivalent to that of 10^6 fluorophores, and enhanced local electromagnetic fields near the surface of the NP that are responsible for the intense signals observed in all surface-enhanced spectroscopies. This strong SPR extinction band (absorption and scattering) allows detection of AgNPs at picomolar levels (10^{-12} M) by using standard absorption spectrometers or at a zeptomolar (10^{-21} M) sensitivity by using more elaborate detection approaches [21–23].

The optical absorption spectroscopy (OAS) is commonly used for *in situ* monitoring of the synthesis process of AgNPs and to obtain quantitative information. However, AgNPs spectra are sometimes difficult to be interpreted because of the occurrence of blue [24] and red shifts, determined perhaps by either an increase of the particle sizes [14,25,26] and/or their organization in clusters [14,26,27].

4.1. AgNPs size determination by OAS

The first aim of this study was to demonstrate that the OAS might be used to size AgNPs in the size range 20–100 nm, provided that the size polydispersity is limited. Literature offers examples [2S–5S] in which the Rayleigh theory was used to determine the light extinction, but this approximated electromagnetic theory works very well for detection of fine particles only at a fixed wavelength.

When the multipolar expansion terms of the electromagnetic field cannot be truncated to the first (dipolar) term [9,1S], as in the case of the AgNPs, the application of the Mie's theory is more appropriate.

Examples in which the OAS was used to size AgNPs in a restricted size range of 2.3–3.7 nm [28] or 3.8–4.5 nm [29] by fitting the experimental spectra with Mie's theory are present in the literature. However, when particles of larger sizes were considered (10, 55, and 80 nm), the OAS was used only to individuate the maximum of the absorption peaks and to conclude that OAS was not suitable to individuate the single populations when the samples are mixed. The sizes were computed in fact by DLS, AFM and TEM [30].

In this study, the size of the particles were computed firstly by fitting each OAS spectrum of the sodium citrate stabilized AgNPs standards with the Algorithm#1 (§ *SM-2* in SM), considering the size as the variable parameter. The fitting tested different optical constants, computed respectively by Palik [31] and Johnson & Christy (J&C) [32].

The size that determined the best fitting for each suspension was taken as "true", and compared in Table 1 (rows 4–5) with those achieved with other well established sizing techniques (TEM and DLS) [7]. The best fittings were obtained with the silver optical constant tabled by Palik [31] but the fit reliability was dramatically lost for sizes below 60 nm.

To improve the size determination, a number of equidistant particles sizes d (nm), in the range 5–120 nm, was set and by applying the Algorithm#2, two series of SPR_{MAX} (in nm) were calculated using again both the optical constants taken from the literature (Palik [31] or J&C [32], respectively). The two series of computed SPR_{MAX} data were interpolated with cubic polynomials (Figure S-2 and Eqs. S8a-S8b),

which were then resolved to achieve the AgNPs sizes by substituting the SPR_{MAX} measured from the experimental spectra. The sizes

obtained from Eq. (S8a) based on the Palik dielectric constants were halfway to DLS and TEM results (Fig. 1 − full red triangles for Palik and full blue diamonds for J&C optical constants). Since the OAS spectra account for both light scattering and absorption and the OAS measurements were done without using polarized light, the deviation from the straight line in Fig. 1 obtained through Eq. (S8a), could indicate a partial particles aggregation rather than imprecise determination of AgNPs size, as previously reported for AuNPs [33].

The third approach considered the TEM data the most reliable measured sizes, even if TEM cannot discriminate between isolated and agglomerated particles, unless when using a polymeric matrix to freeze the colloidal status of NPs before deposition on the TEM grids. The SPR_{MAX} were computed with the Algorithm#2 by using the Palik optical constants. Data were fitted with a cubic polynomial, whose expression is:

$$SPR_{MAX}(OAS) = 406.30 - 0.26792d + 0.01291d^2 + 1.27491 \cdot 10^{-5}d^3 \quad (1)$$

As a benchmark, Eq. (1) was used to determine the AgNPs size starting from the SPR_{MAX} values measured on 3 experimental UV–vis spectra (20, 60 and 100 nm) and the agreement with the nominal size was between 13% (for 20 nm NPs) and 1% (for 100 nm NPs).

It is worth to point out that this approach can be applied only to non aggregated AgNPs, as in case of the samples exploited for this study.

4.2. Quantitative SdFFF particle size distributions

The second aim of this work was to get, for the first time, quantitative particle size distributions of AgNPs from a SdFFF analysis by using the common and relatively inexpensive UV–vis detector.

The SdFFF technique sorts the sample components according to their buoyant mass, consequently for compact spherical particles the FFF theory gives the sizes straightforwardly [1,2]. Unless the SdFFF is equipped with an expensive specific element detector, such as ICP-MS or ICP-OAS, the correct evaluation of the particle size distribution PSD, in terms of mass, but now more and more requested in number [34], might result complicated when the UV–vis detector signal has a complex relation with the sample concentration exiting the separation channel. This happens, when the analytes are plasmonic NPs, such as AgNPs or AuNPs.

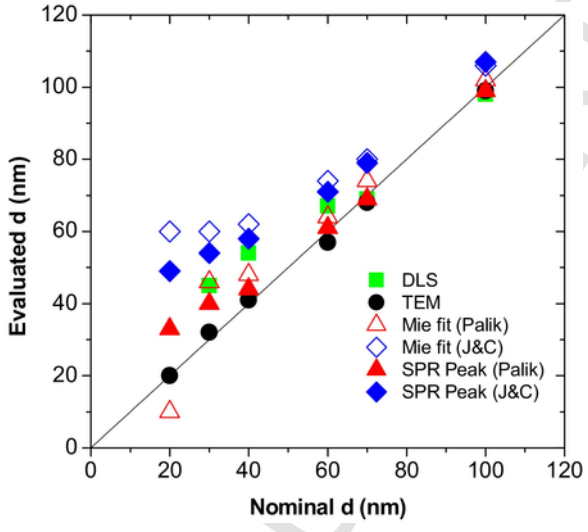

Fig. 1. Measured and evaluated AgNP sizes vs the nominal values. The measurements were done by TEM and DLS, while the computed sizes were evaluated either from the fitting of the UV–vis spectra and the application of the polynomial cubic expressions by using in the Mie algorithms the Palik [30] and the J&C [31] optical constants.

To overcome this difficulty, it is necessary to establish a quantitative relation between the absorbance and the mass of analyte, AgNP with the awareness that the total sample's mass extinction coefficient α_{ext}, in this case, is the sum of the absorption and scattering of light.

The SPR intensity (absorbance *Abs*) is related to Ag atomic concentration (§ *SM*-4 in SM) by the Eq.:

$$c_{Ag} = \frac{1}{MM_{Ag}}\frac{m}{V} = \frac{1}{MM_{Ag}}\frac{m_p}{V}\frac{Abs}{0.434b\sigma_{ext}(d,\lambda)} \quad (3)$$

where MM_{Ag} is the Ag atomic weight, m is the mass of sample, m_p is the mass of the single particle, V is the volume, b is the optical path length and $\sigma_{ext}(d,\lambda)$ is the extinction cross section for the single particle of size d at the experiment wavelength λ.

By adopting the silver optical constants tabled by Palik [31], for which the previous evaluations proved to give results closer to the experimental values than the J&C constants, the Mie's model was used therefore to calculate $\sigma_{ext}(d,\lambda)$. The Algoritm#2 used as sizes those of the standards, while the wavelengths (eight values) were selected between 250 and 440 nm, i.e. in the spectral region going from the plasmon absorption band to the edge of silver interband transitions [12,13,26].

The calculated Ag atomic concentrations (Figure S3) were averaged for each size and compared to the ICP-MS determinations [7] (Table 2, last row). The concentration ranges, computed by considering a single standard deviation around the average, include all the ICP-MS data; however, it is worthwhile to underline that the accuracy and the precision increase with the particle sizes, by reaching the statistical coincidence for the AgNP100 sample.

If the whole set of Ag atomic concentrations data is evaluated instead as a function of the selected wavelengths, it appears that the calculations done at certain wavelengths produce more accurate values then others, almost independently of the particle sizes. Fig. 2, which reports the percentage average error evaluated respect to the ICP-MS data as a function of the used wavelengths, clearly indicates

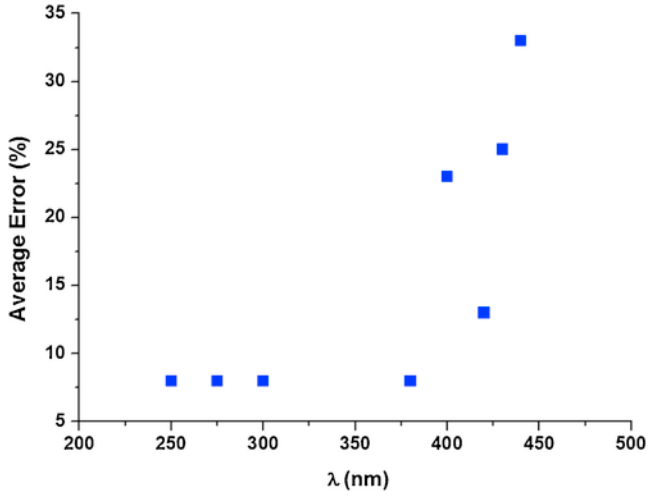

Fig. 2. Percentage average error evaluated for the computed Ag atomic concentrations respect to the ICP-MS data, as a function of the wavelengths used for the AOS measurements.

that the most accurate evaluations are obtained in the 250–380 nm range (7–8%). This is explained by the fact that almost only single-electron interband transitions occur in AgNPs at those wavelengths, and these optical transitions are scarcely affected by particles shape, aggregation and physico-chemical environment, contrary to the SPR [12,13]. However, this point will be further commented in the light of the GF-AAS results, achieved as off-line monitoring of the FFF separations (comment to Fig. 4).

Overall, our findings point out that Mie's theory allowed the accurate and rapid measurement of Ag concentration by optical absorption spectroscopy.

Getting back to the conversion of a fractogram into a correct number PSD, Fig. 3 sketches the steps that this study proposes, in the light of the above results. The raw data (plot (a)) i.e. the UV–vis signal (expressed usually in absorbance units but often in mV or proportional values depending on the acquisition software) are recorded as a function of the retention time (min). In this work, the first detector was set at 420 nm, while the second at 275 nm, 375 nm, 400 nm and 420 nm, as a consequence of the results discussed above. If the UV–vis signal is recorded in volts, the data have to be converted in absorbance units by taking into account the full scale of the detector and the possible applied signal amplification.

The time-axis is transformed in size-axis (diameter) thanks to the FFF software (Analysis) (plot (b)). Because the AgNPs are compact and have a regular spherical shape (see Figure S-4), the diameter can be considered a "real" size. Next, the y-axis (absorbance) is converted into mass concentration by the algorithm based on Mie's theory (Algorithm#3), which uses as input data the particle sizes (x-vector) and the absorbance (y-vector) (plot (c)). It is worthwhile to highlight that the signal recorded at 275 nm was usually the less intense, a fact that will determine an untrustworthy data elaboration. For the sake of objectivity, it must be also recalled that the cleaning condition of the SdFFF channel affects the quality of the signal, determining sometimes an increase of the noise that alters the proportionality among the signal intensities, detected at the different wavelengths. According to the data shown in Fig. 2, the signal recorded at 375 nm should guarantee a reliable conversion in atomic Ag mass concentration. This hypothesis was experimentally verified by monitoring off-line the amount of silver exiting from the FFF channel with a GF-AAS.

Fig. 4 shows the Ag mass concentration profiles elaborated from the UV–vis signal and the actual concentration determined by GF-AAS for the samples of smallest dimensions. The concentration profile computed from the signal recorded at 275 nm has been reported on purpose in all graphs to underline its untrustworthiness, because of the uncertainty on the starting UV–vis signal, as mentioned above. The agreement between the mass of Ag, calculated through Mie's theory, and the GF-AAS experimental element determination was instead quite good for the signals recorded at 375 nm, 400 nm and 420 nm. The best correspondence was found with the signal recorded at 375 nm (see Table S-1).

The number PSDs are eventually calculated for each sample dividing the mass PSD (Eq. S14) by the mass of a single sphere, according the Eq.:

$$F_{n,i} = \frac{6}{\pi d^3 \rho_p} F_{m,i} \tag{4}$$

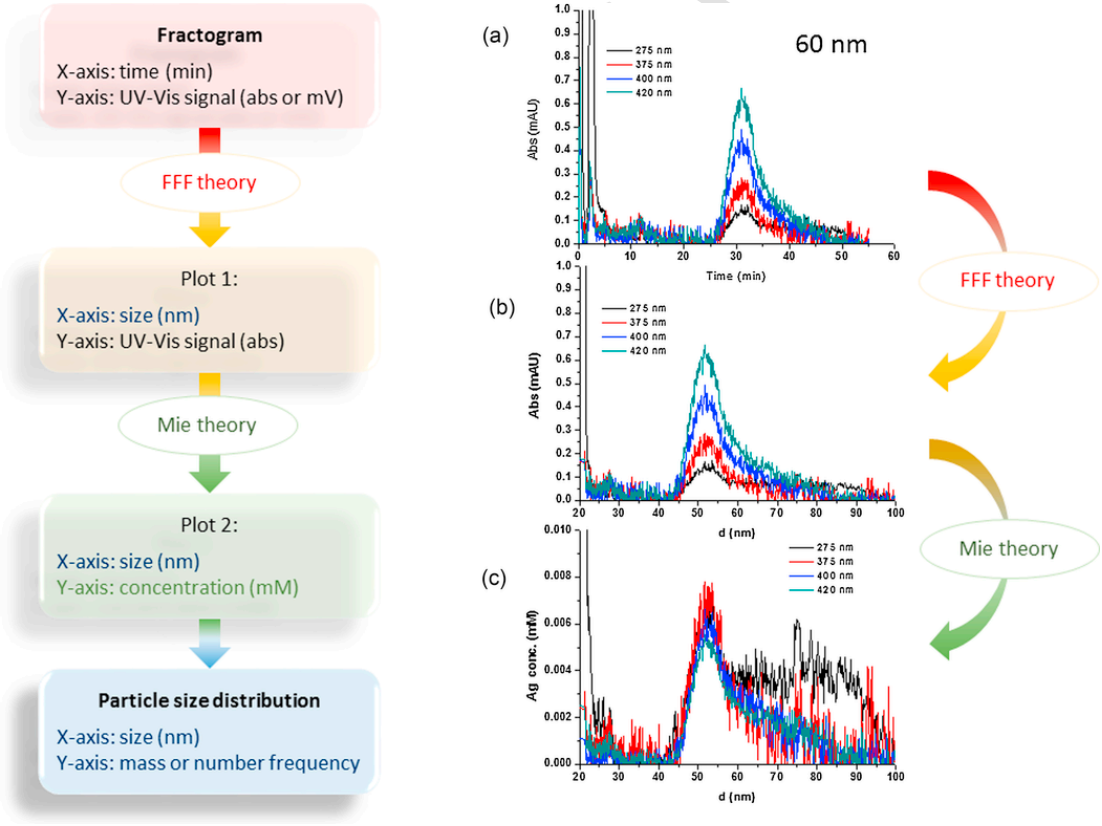

Fig. 3. Scheme of the procedure to transform the fractogram into a number PSD. On the right side of the figure, a practical example applied to the AgNP sample of 60 nm.

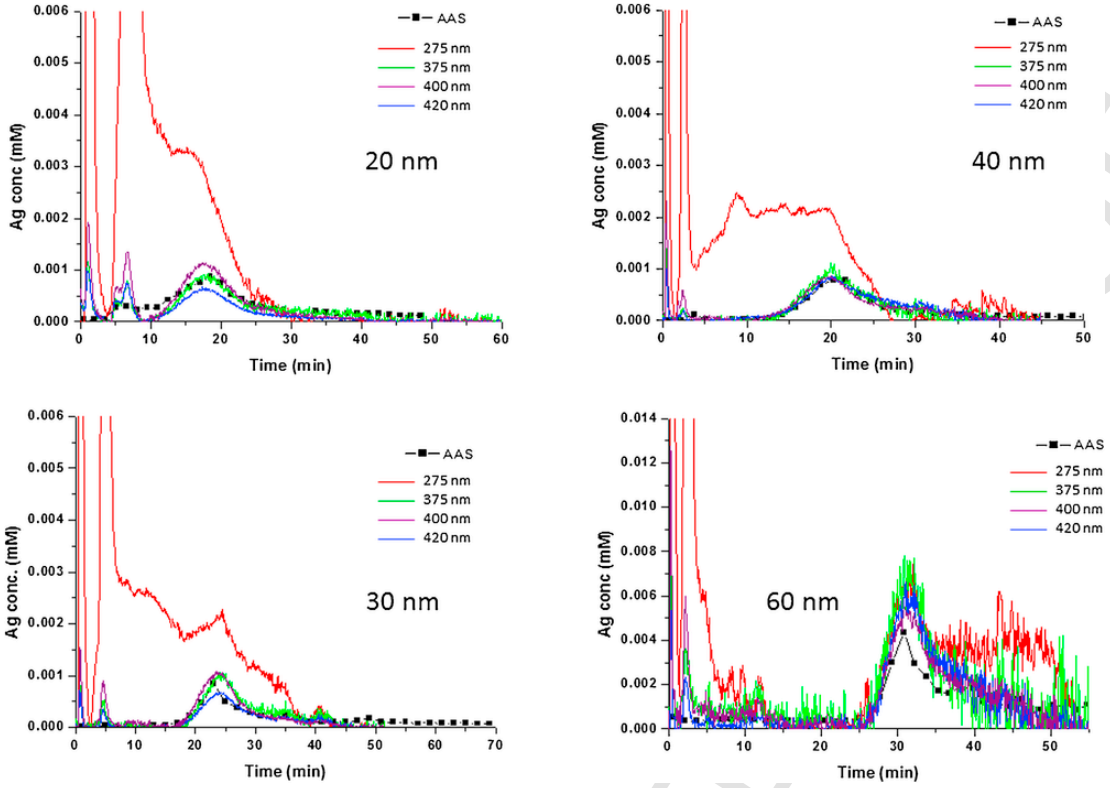

Fig. 4. Comparison between the Ag concentrations (mM) determined from the four UV–vis series of data recorded at 275 nm (red line), 375 nm (green line), 400 nm (purple line) and 420 nm (blue line) and that measured on the eluted fractions by GF-AAS (solid black square). (For interpretation of the references to colour in this figure legend, the reader is referred to the web version of this article.)

Fig. 5 reports, as examples, the number PSDs computed for the AgNP20, 30, 40 and 60 nm samples. The most reliable data are those derived from the signal recorded at 375 nm but for completeness, the PSDs were computed for the four profiles.

As a complement of the above discussion, the GF-AAS data allowed monitoring also the recovery of the separation process. The clean conditions of the SdFFF channel are usually recognized by the absence, or more often, by a limited signal noise. In this case, when the fractions were collected for the GF-AAS measurements, the signal was quite noisy and the recovery confirmed a low separation yield (50–60%).

These last considerations are important in the light of avoiding the use of destructive and expensive elemental specific mass detectors such as ICP-MS or either ICP-OAS, which can give a direct mass or number PSD but paying the price of much higher analysis costs.

5. Conclusions

The results presented in this study prove that monodispersed, spherical, non-aggregate or non-agglomerated AgNPs suspensions can be sized by OAS also when the particle sizes are in the 20–100 nm range. The algorithm, based on Mie's theory and that uses the optical constants tabled by Palik to evaluate the SPR_{MAX} peak position, allows to derive a cubic polynomial fitting equation, that solved respect to the size, gives values in very good agreement with the nominal sizes (relative percentage error of 7%, 1.5% and 0% for the 60 nm, 70 nm and 100 nm samples, respectively). The accuracy worsens only when the dimensions are smaller than 30 nm. The drawback of this approach is the use of the TEM to verify the particle sizes. However, for all those situations, in which the AgNPs are routinely produced and characterized, the use of the time consuming and expensive TEM technique is required only for the initial calibration step.

This study has also proved for the first time that the correct evaluation of the UV–vis signal through Mie's theory, allows to compute mass- and number-sized particle distributions of AgNPs directly from the SdFFF fractograms. This information, so intensely requested nowadays, is achievable without coupling the SdFFF technique with expensive and sophisticated detection units.

The procedure requires to determine first the extinction cross section σ_{ext} of AgNPs and then to use these values to elaborate the raw data produced by the SdFFF, i.e. time and absorbance, and to build trustable PSDs. The agreement between the Ag concentration derived from the UV–vis data, recorded at 375 nm, and the concentration measured by GF-AAS was in some case excellent (-4% - 30 nm) and in some other quite scarce (-23% - 20 nm) not because of the method but rather to the channel cleaning conditions.

The procedures that this study proposes for the AgNPs could be extended also for characterizing gold NPs, provided that the appropriate optical constant are chosen and the limits of the method are experimentally determined. However, because of the required boundary conditions, the applicability of this approach to real samples could have severe limitations.

Conflict of interest disclosure

All authors certify that they have NO affiliations with or involvement in any organization or entity with any financial interest or non-financial interest in the subject matter or materials discussed in this manuscript.

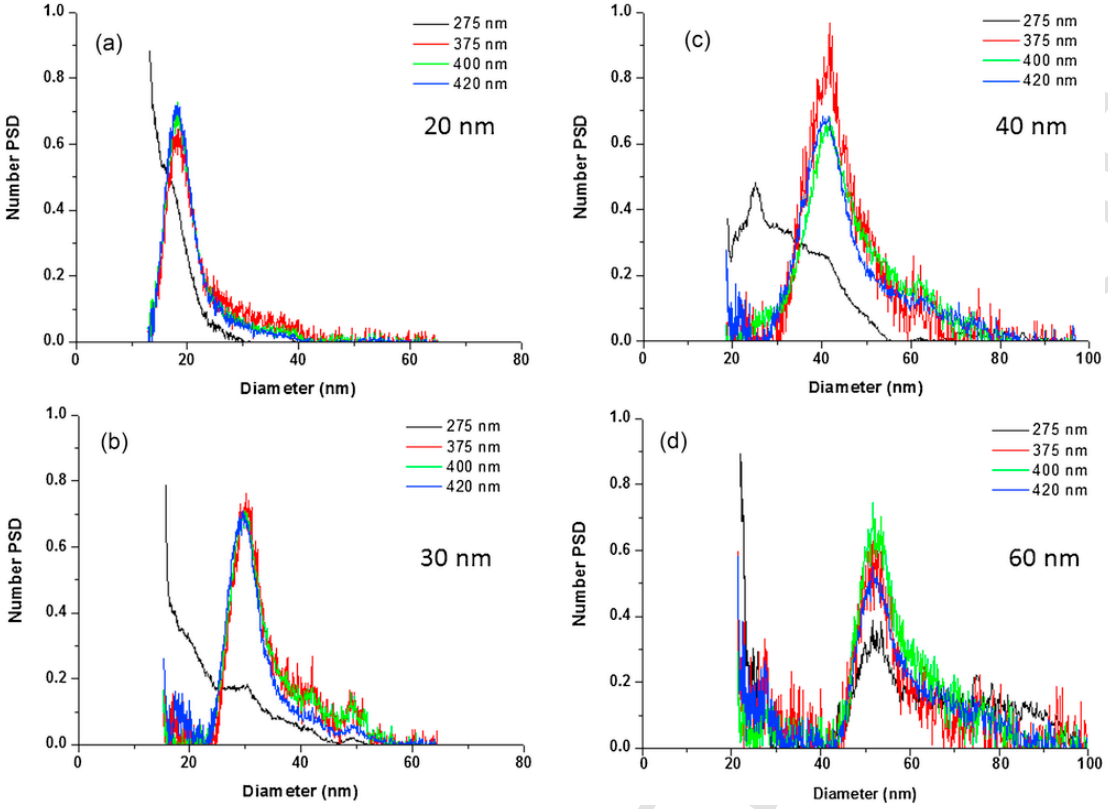

Fig. 5. Area normalized number PSDs computed starting from the UV–vis data recorded at 275 nm (black line), 375 nm (red line), 400 nm (blue line) and 420 nm (green line). (For interpretation of the references to colour in this figure legend, the reader is referred to the web version of this article.)

Acknowledgements

The authors gratefully thank Dr. Antonella Pagnoni for the GF-AAS determinations and the Dr. Daniela Palmeri for her assistance during the TEM observations at the Centro di Microscopia Elettronica of the University of Ferrara.

Appendix A. Supplementary data

Supplementary data associated with this article can be found, in the online version, at http://dx.doi.org/10.1016/j.chroma.2016.10.026.

References

[1] M.E. Schimpf, K. Caldwell, J.C. Giddings, Field Flow Fractionation Handbook, Wiley–Interscience, New York, 2000.
[2] K.R. Williams, K.D. Caldwell, Field-Flow Fractionation in Biopolymer Analysis, Springer, 2012.
[3] C. Contado, R. Argazzi, Size sorting of citrate reduced gold nanoparticles by sedimentation field-flow fractionation, J. Chromatogr. A 1216 (2009) 9088–9098.
[4] L. Calzolai, D. Gilliland, C.P. Garcìa, F. Rossi, Separation and characterization of gold nanoparticle mixtures by flow-field-flow fractionation, J. Chromatogr. A 1218 (2011) 4234–4239.
[5] K. Loeschner, J. Navratilova, S. Legros, S. Wagner, R. Grombe, J. Snell, F. von der Kammer, E.H. Larsen, Optimization and evaluation of asymmetric flow field-flow fractionation of silver nanoparticles, J. Chromatogr. A 1272 (2013) 11116–11125.
[6] O. Geiss, C. Cascio, D. Gilliland, F. Franchini, J. Barrero-Moreno, Size and mass determination of silver nanoparticles in an aqueous matrix using asymmetric flow field flow fractionation coupled to inductively coupled plasma mass spectrometer and ultraviolet–visible detectors, J. Chromatogr. A 1321 (2013) 100–108.
[7] C. Cascio, D. Gilliland, F. Rossi, L. Calzolai, C. Contado, Critical experimental evaluation of key methods to detect, size and quantify nanoparticulate silver, Anal. Chem. 86 (2014) 12143–12151.
[8] A.R. Poda, A.J. Bednar, A.J. Kennedy, A. Harmon, M. Hullb, D.M. Mitrano, J.F. Ranville, J. Steevens, Characterization of silver nanoparticles using flow-field flow fractionation interfaced to inductively coupled plasma mass spectrometry, J. Chromatogr. A 1218 (2011) 4219–4225.
[9] C.F. Bohren, D.R. Huffman, Absorption and Scattering of Light by Small Particles, J. Wiley & Sons, New York, 1983.
[10] F.S. Yang, K.D. Caldwell, J.C. Giddings, Colloid characterization by sedimentation Field-flow fractionation, J. Colloid Interface Sci. 92 (1983) 81–91.
[11] M. Blanda, P. Reschiglian, F. Dondi, R. Beckett, Characterization of low-density polybutadiene latexes by sedimentation field-flow fractionation, Polym. Int. 33 (1994) 61–69.
[12] V. Amendola, O.M. Bakr, F. Stellacci, A study of the surface plasmon resonance of silver nanoparticles by the discrete dipole approximation method: effect of shape, size, structure, and assembly, Plasmonics 5 (2010) 85–97.
[13] C.J. Noguez, Surface plasmons on metal nanoparticles: the influence of shape and physical environment, Phys. Chem. C 111 (2007) 3806–3819.
[14] V. Amendola, M. Meneghetti, Size evaluation of gold nanoparticles by UV–vis spectroscopy, J. Phys. Chem. C 113 (2009) 4277–4285.
[15] J.C. Giddings, F.J.F. Yang, M.N. Myers, Sedimentation field-flow fractionation, Anal. Chem. 46 (13) (1974) 1917–1924.
[16] F.J.F. Yang, M.N. Myers, J.C. Giddings, Programmed sedimentation field-flow fractionation, Anal. Chem. 46 (13) (1974) 1924–1930.
[17] F.J. Yang, M.N. Myers, J.C. Giddings, High-resolution particle separations by sedimentation field-flow fractionation, J. Colloid Interface Sci. 60 (3) (1977) 574–577.
[18] C. Contado, R. Argazzi, Sedimentation field flow fractionation and flow field flow fractionation as tools for studying the aging effects of WO_3 colloids for photoelectrochemical uses, J. Chromatogr. A 1218 (2011) 4179–4187.
[19] J. Ristimaki, A. Virtanen, M. Marjamaki, A. Rostedt, J. Keskinen, On-line measurement of size distribution and effective density of submicron aerosol particles, Aerosol Sci. 33 (2002) 1541–1557.
[20] P.S. Williams, J.C. Giddings, Power programmed field-flow fractionation: a new program form for improved uniformity of fractionating power, Anal. Chem. 59 (1987) 2038–2044.

[21] A.D. McFarland, R.P. Van Duyne, Single silver nanoparticles as real-time optical sensors with zeptomole sensitivity, Nano Lett. 3 (2003) 1057–1062.
[22] C. Batchelor-McAuley, J. Ellison, K. Tschulik, P.L. Hurst, R. Boldt, R.G. Compton, In situ nanoparticle sizing with zeptomole sensitivity, Analyst 140 (2015) 5048–5054.
[23] A. Lapresta-Fernández, A. Salinas-Castillo, S. Anderson de la Llana, J.M. Costa-Fernández, S. Domínguez-Meister, R. Cecchini, L.F. Capitán-Vallvey, M.C. Moreno-Bondi, M.-Pilar Marco, J.C. Sánchez-López, I.S. Anderson, A general perspective of the characterization and quantification of nanoparticles: imaging, spectroscopic, and separation techniques, Crit. Rev. Solid State Mater. Sci. 39 (2014) 423–458.
[24] S. Raza, W. Yan, N. Stenger, M. Wubs, N.A. Mortensen, Blueshift of the surface plasmon resonance in silver nanoparticles: substrate effects, Opt. Express 21 (2013) 27344–27355.
[25] J.J. Mock, M. Barbic, D.R. Smith, D.A. Schultz, S. Schultz, Shape effects in plasmon resonance of individual colloidal silver nanoparticles, J. Chem. Phys. 116 (2002) 6755–6759.
[26] U. Kreibig, M. Vollmer, Optical Properties of Metal Clusters, Springer, Berlin, 1995.
[27] K.L. Kelly, E. Coronado, L.L. Zhao, G.C. Schatz, The optical properties of metal nanoparticles: the influence of size, shape, and dielectric environment, J. Phys. Chem. B 107 (2003) 668–677.
[28] R. Desai, V. Mankad, S.K. Gupta, P.K. Jha, Size distribution of silver nanoparticles: UV–visible spectroscopic assessment, Nanosci. Nanotechnol. Lett 4 (2012) 30–34.
[29] V. Amendola, S. Polizzi, M. Meneghetti, Free silver nanoparticles synthesized by laser ablation in organic solvents and their easy functionalization, Langmuir 23 (2007) 6766–6770.
[30] E. Tomaszewska, K. Soliwoda, K. Kadziola, B. Tkacz-Szczesna, G. Celichowski, M. Cichomski, W. Szmaja, J.J. Grobelny, Detection limits of DLS and UV–vis spectroscopy in characterization of polydisperse nanoparticles colloids, Nanomater (2013) 60–70, http://dx.doi.org/10.1155/2013/313081.
[31] E.D. Palik, Handbook of Optical Constants, Academic Press. Elsevier Inc, 1997.
[32] P.B. Johnson, R.W. Christy, Optical constants of the noble metals, Phys. Rev. B 6 (1972) 4370–4379.
[33] A. Amendola, M. Meneghetti, Size evaluation of gold nanoparticles by UV–vis spectroscopy, J. Phys. Chem. C 113 (11) (2009) 4277–4285.
[34] European Union. Luxembourg 2011. Commission Recommendation of 18 October 2011 on the definition of nanomaterial. Publications Office of the European Union, Official Journal of the European Union [20–10–2011]: L 275/38